Flow Measurement and Instrumentation 52 (2016) 25–39

Contents lists available at ScienceDirect

Flow Measurement and Instrumentation

journal homepage: www.elsevier.com/locate/flowmeasinst

# Simulation-based determination of systematic errors of flow meters due to uncertain inflow conditions

A. Weissenbrunner [a,*], A. Fiebach [a], S. Schmelter [a], M. Bär [a], P.U. Thamsen [b], T. Lederer [a]

[a] Physikalisch-Technische Bundesanstalt (PTB), Abbestr. 2-12, 10587 Berlin, Germany
[b] Technische Universität Berlin, Department of Fluid System Dynamics, Straße des 17. Juni 135, 10623 Berlin, Germany

ARTICLE INFO

*Article history:*
Received 19 February 2016
Received in revised form
14 July 2016
Accepted 31 July 2016
Available online 2 August 2016

*Keywords:*
Pipe flow
CFD
Uncertainty quantification
Venturi
Ultrasonic flow meter
Electromagnetic flow meter
Non-intrusive polynomial chaos
Disturbed inflow profile
Out-of-plane double elbow

ABSTRACT

Computational fluid dynamics (CFD) provides well-established tools for the prediction of the velocity profiles in turbulent pipe flows. As far as industrial pipe and district heating systems are concerned, combinations of elbows are the most common pipe assemblies. Among the different pipe combinations, double elbows out-of-plane are of special interest, since they introduce strong disturbances into the flow profile and have a strong influence on many common types of flow meters. In front of a double elbow there is often another flow-disturbing installation. As a result the upstream conditions are unknown and an investigation of the resulting systematic bias on the measurement of the flow rate and the associated contribution to its measurement uncertainty is necessary. We demonstrate here that this can be achieved by a variation of the inlet profile in terms of swirls and asymmetry components. In particular, an ultrasonic and an electromagnetic flow meter are modeled in order to quantify the systematic errors stemming from uncertain inflow conditions. For this purpose, a generalized non-intrusive polynomial chaos method has been used in conjunction with a commercial CFD code. As the most influential parameters on the measured volume flow, the distance between the double elbow and the flow meter as well as the orientation of the flow meter are considered as random variables in the polynomial chaos approach. This approach allowed us to obtain accurate prediction of the systematic error for the ultrasonic and electromagnetic meter as functions of the distance to the double elbow. The resulting bias in the flow rate has been found to be in the range of 1.5–4.5% (0.1–0.5%) with a systematic uncertainty contribution of 2–2.4% (0.6–0.7%) for the ultrasonic (electromagnetic) flow meter if the distance to the double elbow is smaller than 40 pipe diameters. Moreover, it is demonstrated that placing the flow meters in a Venturi constriction leads to substantial decrease of the bias and the contribution to the measurement uncertainty stemming from the uncertain inflow condition.



## 1. Introduction

Elbow alignments are necessary in almost all pipe assemblies in industrial fields, especially district heating systems. They introduce disturbance to the flow profiles that require a straight pipe length of several diameters to be eliminated. Very often those parts are not sufficiently long to redevelop an ideal profile. Thus, flow rate measurements in ideal flow conditions are not available. It is well known that many flow meters react sensitively to disturbed flow profiles, as they are usually calibrated in ideal conditions at test rigs. To determine these errors an in situ calibration technique with Laser Doppler Velocimetry (LDV), was developed by Müller et al. [31]. The induced errors for large heat meters tested in district heating pipelines are typically higher than 3% and could reach more than 20%, see [14]. In cooperation with TU Berlin, PTB Berlin, ILA GmbH and Optolution Messtechnik GmbH the project "EnEff: Wärme: on-site calibration of flow meters in district heating" [11] was initiated. The idea is to develop a method which permits on-site calibration of installed flow meters in non-ideal installation conditions. A combination of LDV measurements and numerical simulations is desired to predict the flow rate even under problematic inflow conditions.

With a detailed description of the disturbed flow profiles, errors of flow meters can be predicted. Several research activities have taken place to measure flow profiles behind various disturbing pipe installations. Flow profiles following different standard flow disturbers have been studied with particle image velocimetry (PIV) by Eichler [8] and with LDV by Wendt et al. [42]. Yeh and Mattingly performed studies with LDV of the flow profiles downstream of single and double elbows as well as a generic header, tube bundles and t-junctions and showed the effect on the error shifts of turbine and orifice meters [27,28,50–52]. The

* Corresponding author.
*E-mail address:* andreas.weissenbrunner@ptb.de (A. Weissenbrunner).

http://dx.doi.org/10.1016/j.flowmeasinst.2016.07.011

generic header and the double elbows out-of-plane have been detected to produce the highest errors that only slowly subside after several tenths or even more than 100 diameters of straight pipe. Also Wendt et al. and Mickan et al. [30,43] determined error shifts behind single and double elbows out-of-plane for turbine gas meters. Ultrasonic flow meters have been studied experimentally in [5,22,39] and Electromagnetic flow meters in [4,15,19,35]. Depending on the disturbing geometry, the number and arrangement of the ultrasonic paths several percentages of error were determined. Modeled ultrasonic and electromagnetic flow meters were studied by Halttunen [10], where the LDV data of [22] after single and double elbows out-of-plane were used. The double elbows out-of-plane showed the highest errors up to almost 10% for the ultrasonic and about 2.5% for the electromagnetic flow meter.

Due to the cost involved in experimental measurements, they are typically carried out for a few special cases. Numerical simulations are an alternative tool to get an inside into the behavior of the three dimensional flow field. Consequently, ultrasonic flow meters can be modeled by computational fluid dynamics (CFD). For this purpose Eddy viscosity Reynolds-averaged Navier–Stokes (RANS) method are shown to be sufficient, see [17,18]. Tawackolian [39] found out that for ultrasonic meters with several wetted transducers in huge cavities scale resolving transient simulations are necessary.

As the aim of error studies is mostly to correct the flow meter reading, there have been several investigations to improve the measurement values especially for ultrasonic flow meters (USFM). Ruppel [32] developed an error correction procedure based on pressure probes in the flange of the meter to measure the wall shear stress; Yeh et al. [50] proposed a procedure with several ultrasonic paths and flow pattern recognition. Carlander [6] drew a conclusion about self-diagnostics due to the turbulence of the measurement value. There are also two patents [2,10] which claim to have a correction procedure for USFM depending on the distance of the last upstream disturbing installation.

However, all these studies assumed an ideal flow profile before the disturbing geometry. Industrial applications are characterized by high Reynolds numbers. The distance between elbows is typically not sufficiently long to redevelop such an ideal profile. Even if this were so, the flow meter could be installed in front of the elbow. Thus a realistic uncertainty study for flow meter correction must include several elbow combinations. For example, Kn̆ourek [23] simulated several t-junctions and elbows connected behind each other. Usually not every possible elbow configuration can be considered.

To approach the problem in a more general way, in this paper a double elbow out-of-plane is studied with uncertain inflow conditions with CFD, at a Reynolds number of $3{\cdot}10^5$. An uncertainty quantification is carried out by combining two double elbows at random distance and orientation to each other. The statistical quantities for the velocity profiles were calculated by employing the method of polynomial chaos, see Section 2. With this approach, the sensitivity of flow measurements behind a double elbow to uncertain inflow conditions can be quantified and a more general study of flow meters will be presented. Ultrasonic and electromagnetic flow meters are chosen as examples, as they are widely used and their measurement principles are non-intrusive. Moreover, it is shown that a constriction right before the flow meter is to straighten the velocity profile and improves the meter performance considerably. Different shapes of such converging nozzles could be designed to optimize flow conditioning or minimize pressure loss. In this work, two representative designs are studied and proposed: a Venturi nozzle and a rectangular constriction.

The paper is organized as follows: Section 2 briefly describes the concept of uncertainty quantification with polynomial chaos. This approach is applied to a double elbow out-of-plane to study its sensitivity to uncertain inflow conditions. Expected profiles with standard deviations were calculated and compared with measurement results in Section 3. In Sections 4 and 5, these profiles were used to study the error for ultrasonic and electromagnetic flow meters, respectively uncertainties for random angular and axial alignment were calculated. The results were also compared to measurements. Furthermore, expected errors and standard deviations for disturbed inflow profiles to a Venturi nozzle and a rectangular constriction are presented in Section 6. Section 7 provides a summary of the main results and conclusions.

## 2. Concept of uncertainty quantification

A common approach in uncertainty quantification is to use a Monte-Carlo type method. Uses of Monte Carlo methods require large amounts of solutions of the deterministic problem. This becomes an issue when the system is nonlinear and the solution is computationally expensive to obtain such as for problems arising in CFD.

Here, an alternative approach is shortly introduced which is referred to as “polynomial chaos” or sometimes also as “Wiener” or “Wiener–Hermite chaos” in the literature [44]. The idea of the method is to expand random variables with finite second moment in a series of orthogonal polynomials. The method is applicable to a wide range of problems, where the influence of uncertainties within process conditions or variations of material parameters needs to be quantified. In general, the polynomial chaos methods are classified into two approaches: the so-called intrusive methods as well as the non-intrusive ones, see, e.g., [48]. Especially the non-intrusive, sampling based version of polynomial chaos plays an important role when dealing with uncertainties in the context of nonlinear and computationally expensive systems, see [20,25,26,49]. The advantage of the non-intrusive approach is that an existing solver for the underlying deterministic problem can be used as a “black box” without modification. For a more elaborated introduction we refer to [24].

For the introduction of this concept of uncertainty quantification, a physical system

$$\mathcal{L}(x, \xi, g(x, \xi)) = 0,$$

like the incompressible Navier–Stokes equations (4), is considered. Here $g$ denotes some quantity of interest, for example, the velocity field $u$ in Section 3.2 or the volume flow rate in Section 4. Due to uncertain initial or boundary conditions, material parameters, etc., some randomness is introduced in the system. This is modeled by a vector of random parameters $\xi = (\xi_i)_{i=1}^m$ with joined probability density function $p = \prod_{i=1}^m p_i$. The idea of the gPC method is to expand random variables with a finite second moment in a series of orthogonal polynomials, i.e.,

$$g(\xi) = \sum_{i=0}^{\infty} \hat{g}_i \Psi_i(\xi), \tag{1}$$

where $(\Psi_i)_{i=0}^{\infty}$ is a family of orthonormal polynomials with respect to the weighted inner product

$$\left\langle \Psi_i, \Psi_j \right\rangle_w := \int_{\mathbb{R}^m} \Psi_i(s)\Psi_j(s)w(s)ds,$$

with weight function $w$. The family of the orthogonal polynomials and the probability density function of $\xi_i$, $i = 1, \ldots, m$, is connected by the Askey scheme, see [8] and Table 1. In this paper, we only deal with uniformly distributed random variables and therefore

**Table 1**
Correspondence of the family of orthogonal polynomials to the type of probability density function of the random variable. Note that most of the random variables must be scaled in a suitable way such that the corresponding probability density function is equal to the weight function of the polynomial family.

| Distribution | Orthogonal polynomials |
|---|---|
| Gauss | Hermite |
| Gamma | Laguerre |
| Beta | Jacobi |
| Uniform | Legendre |

Legendre polynomials are the appropriate ansatz polynomials.

Exploiting the orthogonality of the ansatz functions, the modes $\hat{g}_i$ of the series expansion are given by

$$\hat{g}_i(x) = \langle g(x,\cdot), \Psi_i \rangle_w, \quad i = 1, \ldots, \infty. \tag{2}$$

Again by the orthogonality of the ansatz, for the expectation $\mathbb{E}(g)$ the variance $\mathbb{V}(g)$ holds

$$\mathbb{E}(g) = \hat{g}_0, \quad \mathbb{V}(g) = \mathbb{E}(g^2) - \mathbb{E}(g)^2 = \sum_{i=1}^{\infty} \hat{g}_i^{\,2}.$$

In practical computations, the degree $d$ of the polynomials has to be restricted, which leads to an approximation

$$g(\xi) \approx \sum_{i=0}^{p} \hat{g}_i \Psi_i(\xi), \quad p+1 = \frac{(d+m)!}{d!m!}, \tag{3}$$

of the series (1). The length $p+1$ of the series increases very fast with the polynomial degree $d$ and the dimension of the random space $m$. This is known as the "curse of dimensionality", see [24], and becomes an issue at least when dealing with problems in a high-dimensional random space. This can be lifted with more sophisticated approaches such as sparse grids, see [13,36]. The convergence property of the truncated series (3) depends mainly on the behavior of the solution of the operator $\mathcal{L}$ with respect to $\xi$. In this paper, the modes (2) are approximated by a tensor Gauss Legendre cubature with nodes $(\xi^j)_{j=1}^q$ and weights $(\lambda^j)_{j=1}^q$, i.e.,

$$\hat{g}_i(x) \approx \sum_{j=1}^{q} g(x, \xi^j) \Psi_i(\xi^j) \lambda^j.$$

This means that the deterministic problem $\mathcal{L}$ have to be evaluated $q$ times, namely at the cubature nodes $(\xi^j)_{j=1}^q$.

## 3. CFD-model of a double elbow

Double elbows out-of-plane and their effects on flow meters have been studied experimentally in [5,22,28,30,32] and numerically in [3,17,18,23,39,53]. The conclusion was drawn that such a geometrical setup generates strong disturbance that causes substantial errors in flow rate measurements. All these investigations assumed ideal flow profiles at the entrance to the double elbow. In an industrial environment this is rarely the case. Moreover, upstream of a double elbow there is typically another installation that creates disturbances. The key question here is, how do the flow conditions upstream a double elbow affect its downstream outcome. To quantify the resulting measurement uncertainty, another double elbow with the same geometry was considered as a disturbance generator upstream of the actual double elbow, see Fig. 1. Additionally, the upstream elbow was reflected at the $xz$-plane, to create an inlet profile with the opposite swirl direction. In order to evaluate the systematic uncertainty contribution, a polynomial chaos study was carried out wherein the distance between the double elbows is considered as a random variable. For a particular application, other parameters such as geometrical parameters of the elbows, valves or diameter jumps might be of greater importance. They can treated analogously as random variables. The aim of the presented study is to give an example of a typical application and not to cover the whole range of (elbow) configurations.

### 3.1. Model and numerical setup

The stationary incompressible Navier–Stokes equations modeling conservation of mass and momentum are given by

$$\nabla \cdot u = 0, \quad u \cdot \nabla u = -\frac{1}{\rho}\nabla p + \nu \Delta u. \tag{4}$$

Here, $u = (u_x, u_y, u_z)^T$ is the velocity field with the secondary components $u_x$,$u_y$ and the axial component $u_z$, $p$ the pressure, $\rho$ the density of the fluid, and $\nu$ its kinematic viscosity. Standard no-slip boundary conditions on the walls and a zero-gradient boundary condition at the outlet are prescribed. At the inlet, a fully developed profile with associated turbulence data is used as a natural inflow boundary condition (for details see below). The turbulent flow of water in a pipe with an inner diameter $D$=53.6 mm is considered. The straight pipe downstream of the double elbow has a length of 50 $D$. The geometry of the setup is shown in Fig. 1. The volumetric velocity is fixed to be $u_{vol} = 4.19\ \mathrm{ms}^{-1}$, which corresponds to a Reynolds number of about $\mathrm{Re} = 3{\cdot}10^5$. In order to perform the numerical simulations in this setup, the commercial CFD solver ANSYS CFX was used. The Reynolds-averaged Navier–Stokes (RANS) equations were solved with the closure model $\kappa - \omega$ from Wilcox [45], which shows the best results among eddy viscosity models in a pipe flow [39,40]. A hexahedral mesh consisting of 3.2 million elements with a non-dimensional wall distance $y^+ \approx 1$ was used. The mesh was created using the O-grid technique with the tool ANSYS ICEMCFD.

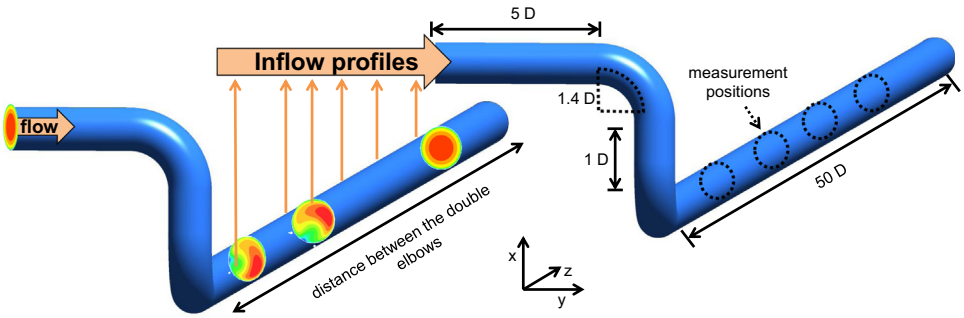


**Fig. 1.** The setup of the numerical experiments with two double elbows in a row, with variable distance in between.

### 3.2. Simulation results

The development of the velocity profile downstream of a double elbow out-of-plane was simulated starting with fully developed inflow conditions obtained from a separate simulation of a straight pipe. The profile has a varying asymmetric shape with a swirl whose strength decreases further downstream. About 5*D* downstream of the elbows, a typical sickle-shaped profile can be found. The isosurface representing the maximum velocity rotates in the flow due to the swirl with increasing distance, while the sickle shape slowly disperses.

In the first step, a comparison with experimental measurements is needed to assure that the numerical simulations are suitable. A contour plot of the normalized axial velocity profile $u_z/u_{vol}$ at a distance of 5*D* downstream of a double elbow from experimental data measured with particle image velocimetry (PIV) from Optolution Messtechnik GmbH[1] is shown in Fig. 2a, compared with a CFD simulation, Fig. 2b. In both, a typical sickle shape can be obtained. Even if the sickle shape is more pronounced in the simulation, it captures the main qualitative effects seen in the experiment. The arrows show the direction $\left(u_x, u_y\right)^T$ and the magnitude $\frac{1}{u_{vol}}\sqrt{u_x^2+u_y^2}$ of the swirl. In the experiment and the simulation a single swirl in counterclockwise direction with similar magnitude is obtained. The swirl center lies southeast of the center of the cross section. Note that the measured values near the wall are superposed by reflections. The measured profile was obtained at a different Reynolds number $2{\cdot}10^5$ and with a slightly different diameter (54.4 mm). The flow profile before the double elbow was fully developed.

The velocity and turbulence profiles from the simulation with a fully developed inlet profile at 20 different planes with different axial positions were used to define the inlet conditions for 20 additional simulations. Another 20 simulations were performed with the reflected profiles as inlet conditions, in order to change the swirl direction.

The normalized axial velocity profile 5*D* downstream of the last elbow with disturbed inlet conditions is shown in Fig. 2c and d. The profiles still exhibit the typical sickle shape. Depending on the inlet conditions their azimuthal orientation varies. If another double elbow with the same swirl direction is considered as inflow condition, the swirl is enhanced, which causes the sickle shape to turn faster. With inflow conditions 12*D* downstream of the double elbow, the sickle has already turned further (in counterclockwise direction) about 60°, compared with the fully developed inlet case, see Fig. 2c. For the inflow profile 12*D* downstream of the double elbow with the opposite swirl direction, the swirl is weakened and the axial velocity profile has turned about 60° less than the profile with fully developed inlet conditions; also the shape of the sickle is less sharp, since the strength of the swirl influences the redevelopment of the profile, see Fig. 2d. From the gray scale of the arrows the weakened/enhanced magnitude of the swirl can be obtained.

To quantify the uncertainties caused by the variations of the inflow profiles, the distance of the double elbows from each other was defined as a uniform distributed random variable $\xi \in [5, 48]\, D$. In this study, 20 sample positions were used. This allows an approximation with polynomials up to the degree 19. The detailed sample positions follow from the roots of the polynomials. Two polynomial chaos studies were performed: in the first study ($T_1$) the two elbows have the same orientation, whereas in the second study ($T_2$) the orientation of the second elbow is mirrored. With the orientation as a discrete random variable, the two calculations can be combined [34] and the expectation and variance can be calculated by

$$E(T) = \frac{1}{2}\big(E(T_1) + E(T_2)\big); \quad V(T) = \frac{1}{2}\big(V(T_1) + V(T_2)\big) + \frac{1}{4}\big(E(T_1) - E(T_2)\big)^2. \tag{5}$$

Fig. 3a and b show the expected axial velocity profile. The corresponding standard deviation $\mathrm{Std} = \frac{100}{U_{vol}}\sqrt{V(Z)}$ in % is shown in Fig. 3c and d. Fig. 3a and b are computed, at the cross section in a distance of 5*D*, and Fig. 3b and d in a distance of 17*D* downstream of the last elbow. While for the closer cross section the expected profile still exhibits a sickle shape, the profile at a distance of 17*D* downstream is almost rotationally symmetric. Note that the symmetry is caused by averaging over the different inlet positions. For each inlet position, the resulting profile is still sickle shaped. The standard deviation at a distance of 5*D* downstream shows a relative localized maximum value of 10%, with lower values where the sickle is expected. Further downstream the standard deviation is spread increasingly over the cross section with values up to 9% and shows a minimum around the center area.

In conclusion, especially for fully developed inflow conditions the simulated profile well agreed with the measured one. With respect to error prediction of flow rate measurements not only the last disturbing installation should be taken into account. For several disturbing installations connected in series, which can be found in many pipe assemblies, an accurate prediction of the flow profile and, thus, an accurate error estimation for a flow meter is more challenging. In the following sections, ultrasonic and electromagnetic flow meters are studied.

## 4. Uncertainty of an ultrasonic flow meter

The disturbed flow profiles from the previous section are now considered as inflow profile of a modeled flow measurement device. An ultrasonic flow meter (USFM) is studied first, as it is expected to be sensitive to disturbances [5,9,22,39]. The measurement principle of an ultrasonic single-path flow meter is therefore modeled. Thus, the velocity field is transformed into a cylindrical coordinate system $(r, \phi, z)$, with the velocity vector $u = (u_r, u_\phi, u_z)^T$.

### 4.1. Measurement principle

There are several types of ultrasonic flow meters on the market. The two main measurement principles are the Doppler and the travel-time techniques. Here, the dual sensor travel-time technique will be discussed. Two sensors ($A$ and $B$) are situated inside or outside the pipe wall, see Fig. 4. Each sends and receives ultrasonic impulses that propagate through the fluid. The time between sending and receiving from one to the other sensor is measured. It can be written as

$$t_{AB} = \frac{L}{C + \bar{u}_p e_z}, \quad t_{BA} = \frac{L}{C - \bar{u}_p e_z}, \tag{6}$$

where $C$ denotes the speed of sound in the fluid, $\bar{u}_p$ the mean velocity along the ultrasonic path, and $e_z$ the $z$-component of the unit vector $e = \big(\sin(\alpha), 0, \cos(\alpha)\big)^T$ tangential to the path. The measurement value $\bar{u}_p$ can be determined by

$$\bar{u}_p = \frac{L}{2e_z}\left(\frac{1}{t_{AB}} - \frac{1}{t_{BA}}\right).$$

[1] Experimental data obtained by Ulrich Müller, Optolution Messtechnik GmbH, internal campaign 2014.

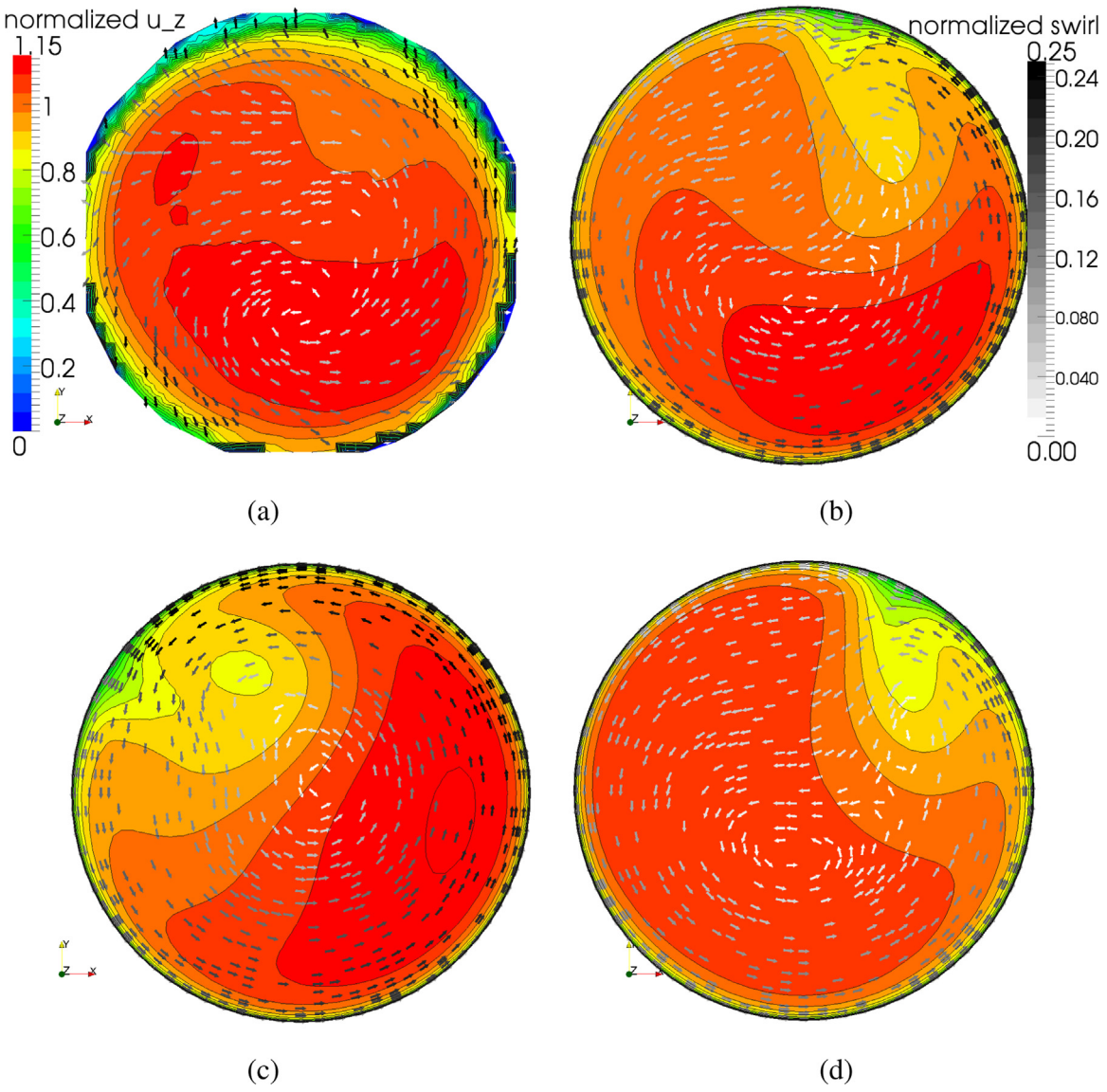


**Fig. 2.** Comparison of the axial velocity profile normalized with the volumetric velocity $u_{vol}$ 5*D* downstream a double elbow with different inlet conditions. With fully developed inflow, by particle image velocimetry (PIV) measurements[1] (a) and a CFD simulation (b). With disturbed inflow conditions from 12*D* downstream of a double elbow with the same swirl direction (c) and with opposite swirl direction (d). The arrows show the secondary flow components, the normalized magnitude is visualized by their gray scale.

There are different approaches to model an ultrasonic beam traveling between the transducers. Here, the ultrasonic beam is assumed to be a straight-line. This means a simplification, because the acoustic path is curved, due to the flow and temperature profile. Yeh and Mattingly [53] have shown that this effect is sufficiently small for Mach numbers <0.1. With a ray tracing approach, Iooss et al. [21] showed that the flow rate is overestimated up to 2% by this model simplification even for fully developed profiles, when turbulent and thermal effects are concerned as well. Furthermore, the ultrasonic beam has a spatial expansion. The sound beam can therefore be modeled as an elliptic volume, see [18]. For small pipe diameters this should be considered, but it is neglected in this work. If the USFM is an in-line meter, the transducers are situated in cavities inside the pipe or extend into the pipe, which causes additional effects, see [39]. Also different path assemblies can be considered which might improve the measurement results, for example see [17]. Here, for demonstration of the method, a non-intrusive single beam with straight line wave propagation is considered.

Since the mean velocity of a path is not the same as the mean velocity over the cross section, $\bar{u}_p$ has to be multiplied by a calibration factor $k = u_{vol}/\bar{u}_p$. Since the real flow profile in a pipe system is unknown, the ratio $k$ is usually calculated for a fully developed flow profile. If the flow profile is disturbed particularly, not rotationally symmetric, the calculated value for $k$ is wrong, which depicts the first source of error. The second one is caused by non-axial/cross velocity components, since the ultrasonic impulse is not only driven by the axial velocity component $u_z$, as the angle $\alpha$ (practically) cannot be zero. With a cylindrical coordinate system, only the radial component $u_r$ disrupts the measurement value, since $u_\phi$ is orthogonal to the vector $e$. The mean velocity can then be calculated as

$$u_{vol} = k\bar{u}_p = \frac{k}{Le_z}\int_0^L u(l)e\, dl. \tag{7}$$

For an ideal flow profile with no secondary flow components the correct value of the mean axial velocity $\bar{u}_z$ can be determined. For the presented results, the axial angle $\alpha$ is fixed at $\pi/4$. The analytical velocity distribution of Gersten and Herwig [12] differs slightly from the CFD simulated profiles. Therefore, the calibration factor $k=0.949$ is calculated by the velocity profile obtained by an additional CFD simulation of a more than 100*D* long straight pipe. The obtained

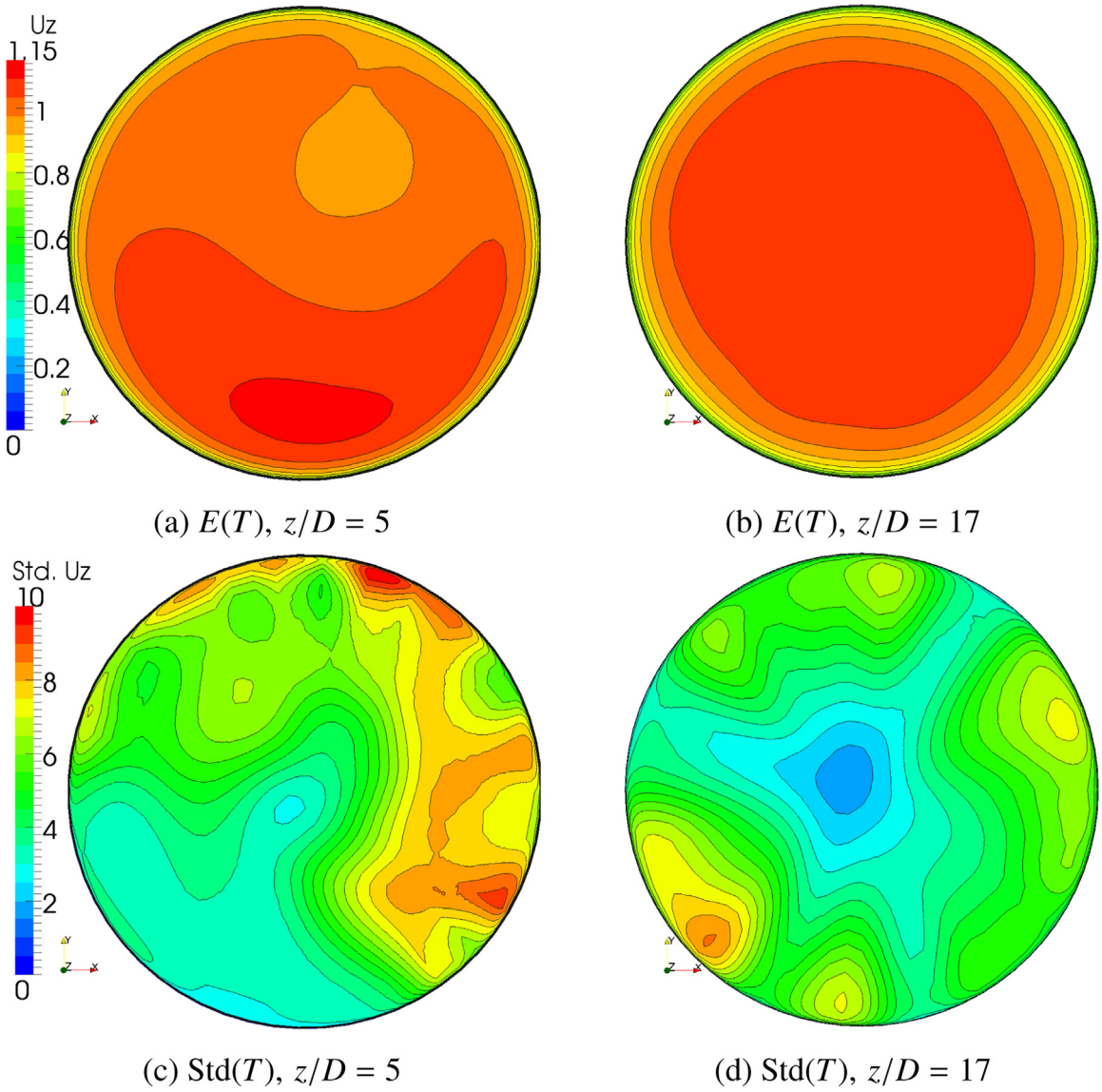


**Fig. 3.** Statistical quantities due to random distance and orientation between two double elbows. The expected normalized axial velocity profile (a) 5*D* and (b) 17*D* downstream of the second double elbow and the related standard deviation in % (c) and (d).

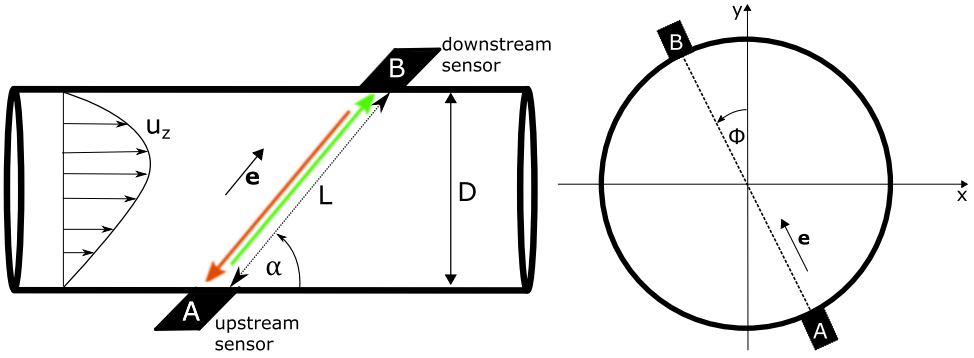


**Fig. 4.** Principle of an ultrasonic flow meter construction.

profile is a more suitable reference for comparisons with CFD simulated disturbed flow profiles.

### 4.2. Results

The relative error of the simulated flow meter in percent is given by

$$\varepsilon = \frac{100}{Q_{real}}(Q_m - Q_{real}), \tag{8}$$

where $Q_m$ is the flow rate from the meter and $Q_{real}$ is the exact flow rate. The following cases were studied:

(i) Two identical double elbows in a row at a random distance

from each other.

(ii) Two identical double elbows in a row at a random distance from each other; first double elbow is reflected on the *xz*-plane.

(iii) Combination of Cases (i) and (ii) with joint statistics, calculated using (5).

(iv) One double elbow with ideal inflow conditions and random angular alignment of the flow meter $\phi$, as defined in Fig. 4. To calculate the standard deviations with polynomial chaos 20 angular positions $\phi \in [0, 2\pi]$ were used.

The Cases (i) and (ii) reflect a situation where the installation elements in front of the flow meter are known in detail except for the distance between them. In some cases, the combination of the installation elements may not be known so that a statistics over possible constellations is needed – this situation is considered here in Case (iii). In Case (iv), it is assumed that several installations may affect the flow before it enters the double elbow in front of the flow meter and that therefore the angle of the orientation of the asymmetric flow profile entering the meter is unknown. This is modeled here by assuming a random angle of the flow meter. While this selection of cases will not capture every possible situation, it will allow to us obtain a comprehensive overview of the magnitude and variation of systematic biases caused by well-specified or (partially) unknown installation in the flow track before the meter. Since the results, depend strongly on the distance of the flow meter to the double elbow, we usually show their dependence on this parameter. In order to enable an easier comparison between the different Cases (i)–(iv) and also to allow an easy assessment of the effect of elements that compensate the systematic effects on the flow measurement (see Section 6 below), results for the bias and the systematic uncertainty contribution were also averaged over a specified range of distances and are provided in Table 2.

For an angular position of $\phi = 0$, the expected error for the Cases (i)–(iii) over the distance to the last elbow starts at a value between $-3$ and $-6\%$ at a distance of $5D$ and decreases, oscillating towards about 1% at a distance of $47D$ to the last elbow. The standard deviation decreases from about 3% towards 1.5% and also oscillates slightly, compare Fig. 5a–c. For Case (iv) the outlet of the double elbow has a length of $100D$. The expected systematic error decreases asymptotically from $-4\%$ towards zero. The standard deviation is about 2.5% near to the elbow and decreases slowly to about 2% at a distance of $50D$. From there on, it decreases more rapidly to a small value of 0.4% at a distance of $94D$. The minimum and the maximum deviation decrease from $-6\%$ and $+3\%$ to $\pm 0.5\%$ respectively, see Fig. 5d. It can be seen that Case (iv) approximates the statistics of the other cases quite well. The expected error for Case (iv) with random position and random angular alignment of the USFM was calculated to be $-1.42\%$ with a standard deviation of 0.7%, see Table 2.

**Table 2**
Calculated uncertainties downstream a double elbow with a random distance of 5–$100D$ and random angular position $\phi \in [0, 2\pi]$ of the simulated flow meter. Results are given for the cases without constriction, with a Venturi nozzle and a rectangular constriction. For explanation see Sections 4 and 5.1.

| | USFM | | | EMFM | | | Unit |
|---|---|---|---|---|---|---|---|
| Flow rate | No constr. | Venturi | Rect. | No constr. | Venturi | Rect. | |
| $Q$ exact | 34.08 | 34.08 | 34.08 | 34.08 | 34.08 | 34.08 | $m^3/h$ |
| Expectation value | 33.63 | 34.05 | 33.70 | 33.98 | 34.05 | 34.04 | $m^3/h$ |
| Expected error | −1.34 | −0.11 | −1.14 | −0.31 | −0.10 | −0.10 | % |
| Standard deviation | 0.70 | 0.34 | 1.12 | 0.17 | 0.02 | 0.01 | % |

The proposed uncertainty study is tested by comparing the outcome with earlier results of Halttunen [16]. The data were re-digitalized in order to show it in the same plot. The data were generated by applying the same modeling approach of a single beam USFM as used in this work, see Section 4.1. But instead of results from CFD simulations, velocity profiles downstream of a double elbow out-of-plane from laser-Doppler-velocimetry (LDV) measurements of the US National Institute of Standards and Technology (NIST) [27] were used. The Reynolds number of the measurements was $10^5$, and thus three times lower than in this work ($3 \cdot 10^5$). Nevertheless the results were plotted together with the approach from Case (iv) in Fig. 5d. The triangles are the errors for an angular alignment of $\phi = 0°$ and $\phi = 90°$. The same trend of the experimental and the simulated results can be obtained. Most points are within the standard deviation (red error bars) and are gathered around the expected error (cyan line) and therefore in line with the results of our study. A single point close to the elbow exit is outside the standard deviation but still inside the minimum deviation (blue error bars). Only three values from [27] obtained at a distance larger than $90D$ downstream differ from the uncertainties obtained in this investigation.

The propagation of the error depending on the distance and the angular alignment of the USFM is shown in Fig. 6a. Nearly periodic structures can be seen in both directions, where the amplitudes decrease with axial distance to the elbows. The change over the angular alignment $\phi$ in $32D$ is shown in Fig. 6b. The interpolation by the Legendre polynomials (red) captures the values of extrema that would be underestimated by the sampling points (blue). The expected error at this cross section is depicted in black dots and the expected error plus and minus the standard deviation is shown in green lines.

It can be concluded that the simulated CFD profiles are suitable for predicting errors of USFM downstream a double elbow out-of-plane. The calculated standard deviations are a good approximation of the systematic contributions to the uncertainties of an USFM that stem from installation effects such as the uncertain inflow profile and the position of the flow meter behind the elbow.

## 5. Uncertainty of an electromagnetic flow meter

The influence of installation effects and the resulting systematic uncertainties in the performance of an electromagnetic flow meter (EMFM) is studied in this section. The approach is analogous to the one applied to the ultrasonic flow meters in the preceding section. Error shifts of an EMFM were previously studied in [1,4,15,16,19]. An EMFM seems to be much less sensitive to disturbed flow profiles than the USFM considered in the last section. EMFMs are also considerable more expensive than USFMs, which make them only applicable where they promise a substantial extra benefit in measurement accuracy. Yet they are not free of errors for disturbed inflow profiles, which is due to their measurement principle, which will be explained in the following section.

### 5.1. Measurement principle

Electromagnetic flow meters rely on the generation of a measurable potential difference in the (conducting) fluid by its motion through a transverse magnetic field [35]. For a pipe with a circular cross section two electrodes A and B are usually placed on the pipe walls perpendicular to the magnetic field, see Fig. 7. Under the assumption that the axial velocity $u_z$ vanishes at the wall and the walls are not conducting, the flow rate $Q_m$ can be determined by the potential difference between the points A and B, see [35],

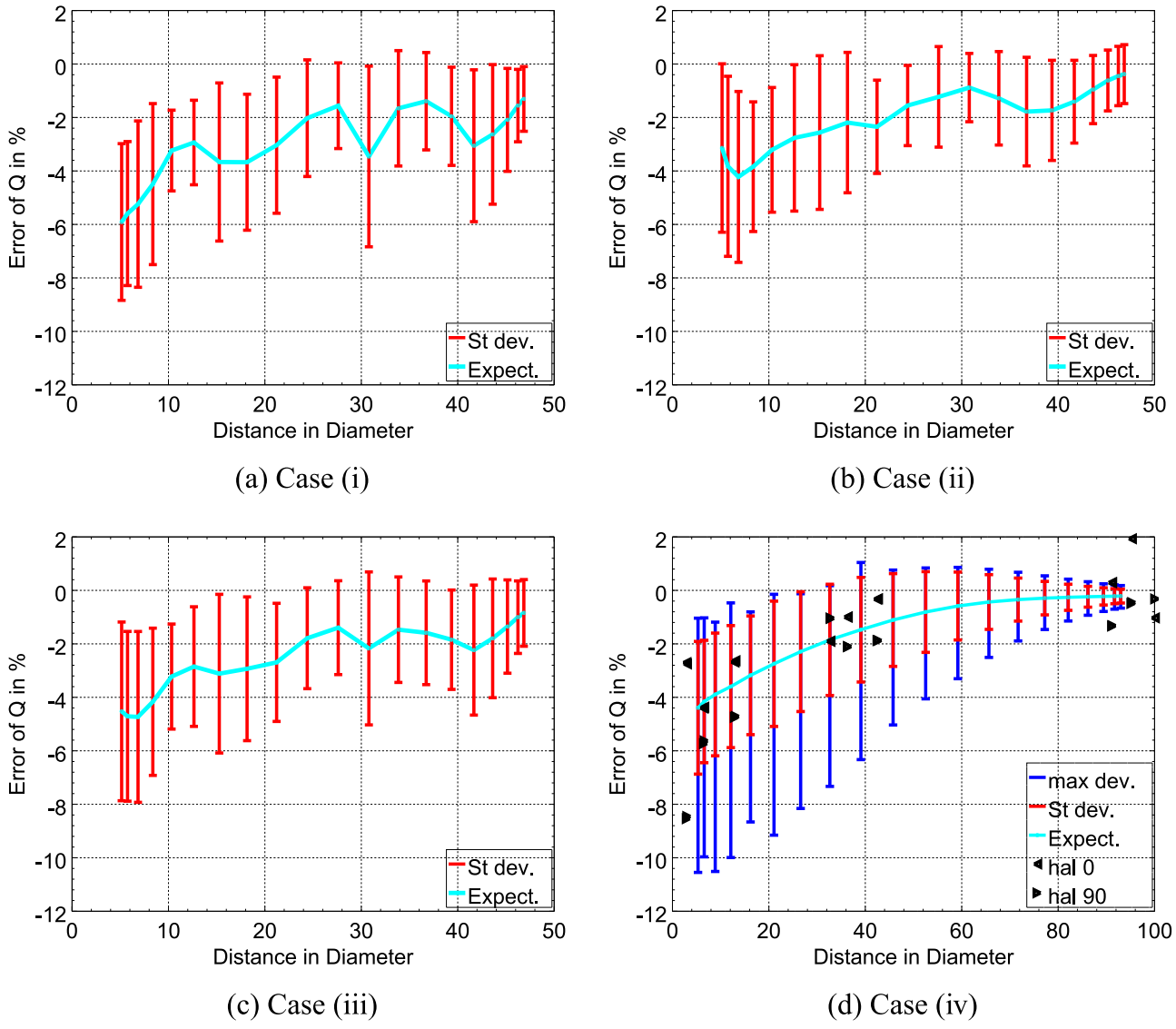


**Fig. 5.** The expected error of an USFM and its standard deviation over the distance to the last elbow. For (a), (b) and (c): with a fixed angle of $\phi = 90°$ and the distance of the first double elbow as random variable with the same swirl direction (a), with the opposite swirl direction (b), both combined (c). The double elbow with fully developed inflow conditions with a random angular position of $\phi$ (d). The error bars in red denote the standard deviation, in blue the max and min deviation at each position. Note that the horizontal axis in (d) is twice as long as in the others. The black triangles represent digitalized experimental data from Halttunen [16], with an angle of 0° and 90°. (For interpretation of the references to color in this figure caption, the reader is referred to the web version of this paper.)

$$Q_m = \iint_{\Omega} u_z(x, y) W(x, y)\, dx\, dy, \tag{9}$$

where $\Omega$ denotes the cross section of the pipe. The weighting function $W$, which is also known as the Shercliff function, is given by

$$W(x, y) = \frac{R^4 + R^2(x^2 - y^2)}{R^4 + 2R^2(x^2 - y^2) + (x^2 + y^2)^2}, \tag{10}$$

and depicted in Fig. 7. Note that the Shercliff function has singularities at the position of the electrodes. Here the positions of the electrodes are located at $(-R, 0)$ and $(R, 0)$, see Fig. 7. To apply the weight function for our purposes, it is cut off at a value of 2.5.

In [37], weight functions for other configurations, for example for rectangular flow meters, can be found. To get the desired quantity of the flow rate, the measured value $Q_m$ has to be multiplied by a calibration factor $k = 1.05$, which was calculated for a fully developed flow profile, similar to the approach explained in Section 4. If the shape of the velocity profile is not fully developed, particularly non-symmetric, the measurement value will be biased.

### 5.2. Results

The investigation of the EMFM covers the Cases (i)–(iv), which are the same as in Section 4.2. The only difference is, that the USFM is now replaced by an EMFM. For an angular position of $\phi = 0$, the expected error for Cases (i)–(iii) over the distance to the last elbow starts at about $-0.4$ to $-0.7\%$ at a distance of $5D$ and decreases in an oscillating manner towards zero at a distance of $47D$ to the last elbow. The standard deviation also oscillates slightly, but hardly decreases, and varies in the range 0.3–0.7%, compare Figs. 8a, b and c. For Case (iv) the outlet of the double elbow is $100D$. The expected error decreases asymptotically from $-0.5\%$ towards zero. The standard deviation is about 0.6% at $5D$ and hardly decreases until $50D$; at position $94D$ the standard deviation is about 0.1%. The minimum and maximum deviations decrease from $-1\%$ and $+0.8\%$ to $\pm 0.1\%$ respectively, see Fig. 8d. As for the USFM, it can be seen that Case (iv) approximates the statistics of the other cases quite well. The expected error for Case (iv) with random position and random angular alignment of the

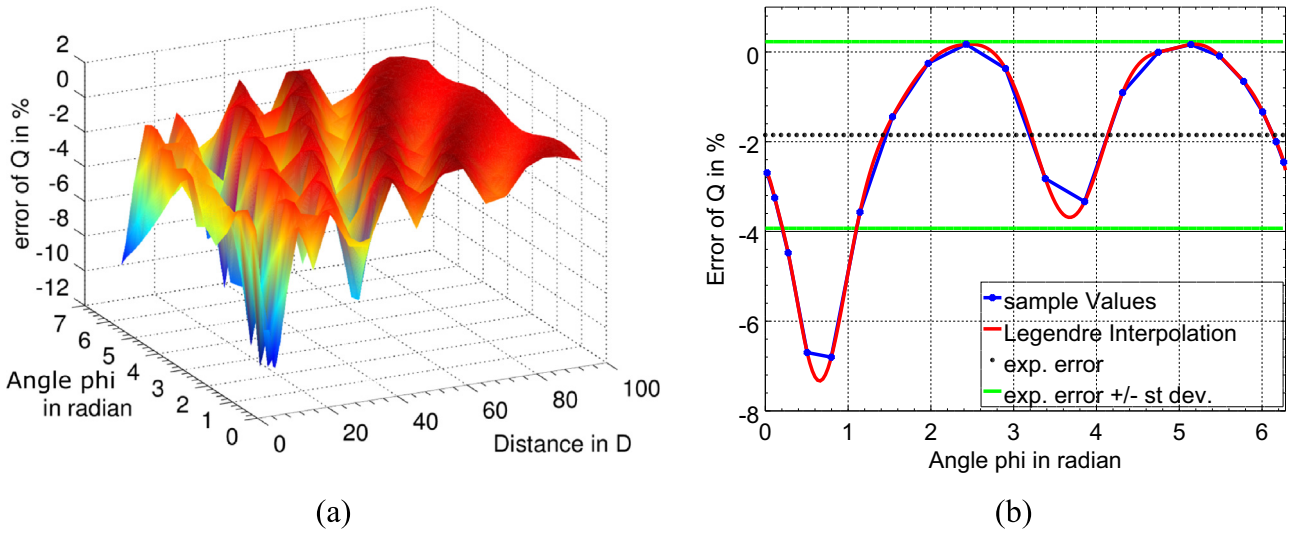


**Fig. 6.** The flow meter error plotted vs. angular and axial position of the flow meter (a) and over the angular position of the flow meter at the axial position 32*D* (b), the sampled values with piecewise linear connection in blue, the Legendre interpolation in red, the expected error in the dotted black line and the expected error ± the standard deviation for this cross section in green. (For interpretation of the references to color in this figure caption, the reader is referred to the web version of this paper.)

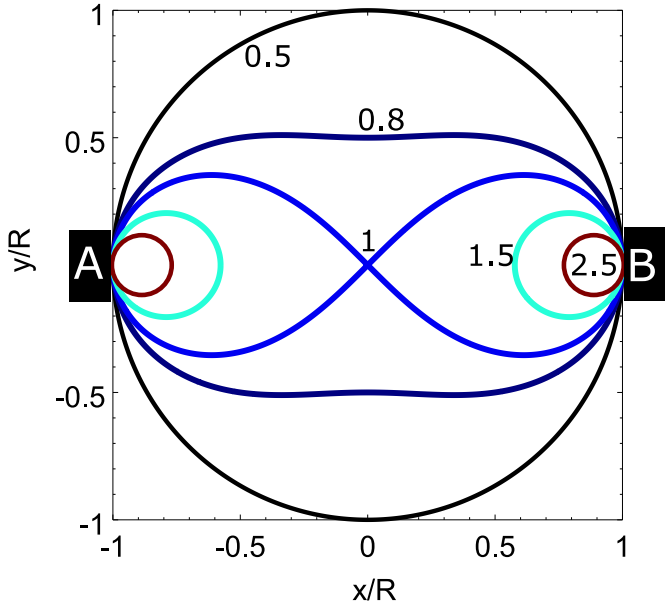


**Fig. 7.** Contour lines of the Shercliff function of an EMFM in a cross section of a circular pipe.

EMFM was calculated to be −0.31% with a standard deviation of 0.17%, see Table 2. Therefore the expected error and the standard deviation of an EMFM are smaller by a factor of 4 than for a single path USFM. To check the simulation results they are compared with experimental data obtained at FORCE Technology.[2] Two setups were considered. In the first setup, the volume flow rate is measured by an EMFM at three distances (0, 10, and 27*D*) behind a double elbow out-of-plane. For the second setup, a clockwise swirl generator is additionally put in front of the double elbow. The measurements were performed at a temperature of 24 °C and a pressure of 1.5 bar. The volume flow rate was about 34.1 $m^3/h$, which corresponds to a Reynolds number of about $3{\cdot}10^5$. The measurements were repeated five times with about 23,000 pulses each in about 240 s. The geometry of the elbows used in the experiments differs from the one used for the above simulations. The distance between the elbows is smaller, as they are directly mounted together. For a better comparability, an additional simulation was carried out with the geometry used in the experiments. Fig. 9 shows the mean values of the resulting relative error of the volume flow rate with respect to a reference flow rate which has been determined by measurements under ideal conditions. The results for the first setup are depicted in green, for the second setup in black. The error bars depict the standard deviation of the five measurements which in all cases is about 2%. The experimental data are plotted within the calculated uncertainties from Case (iv). The cyan line depicts the expected error, the red error bars the standard deviation, and the blue error bars the maximum/minimum errors for variation of the angular alignment at the particular position..

It can be concluded that a priori distortion of the velocity profile influences the outcome of the profiles downstream of a double elbow, since the experiments with a swirl generator before the double elbow differ from those without swirl. The error of the experiments does not decrease significantly for a distance of up to 27*D* downstream of the elbows. The presented uncertainty study proved to be a good approximation, since the estimated errors from the experiment all lie within the predicted standard deviation.

## 6. Influence of constrictions on the disturbance

As shown in the previous sections, the exactness of a flow meter is dependent on the flow profile. In an industrial environment an ideal flow profile is rarely accessible. Nevertheless, exact measurements of the flow rate with as small as possible systematic uncertainty contributions are desired under any circumstances. Thus improvements in the accuracy of the flow meter are needed under disturbed flow conditions.

One possibility to improve the measurement performance is to install flow conditioners right after the disturbing geometry. This causes a destruction of the previous disturbance, but it still requires a length of more than 20*D* of a straight pipe until the ideal flow profile is developed [47]. That makes flow conditioners applicable for test rigs, but hardly in an industrial environment.

A lot of effort has been made to correct the error shift of the meter. Therefore the disturbed profile must be well known. Even if the geometry of the disturbing installation is known, it is hard to

[2] Experimental data obtained by Johan Bunde Kondrup, FORCE Technology, Denmark.

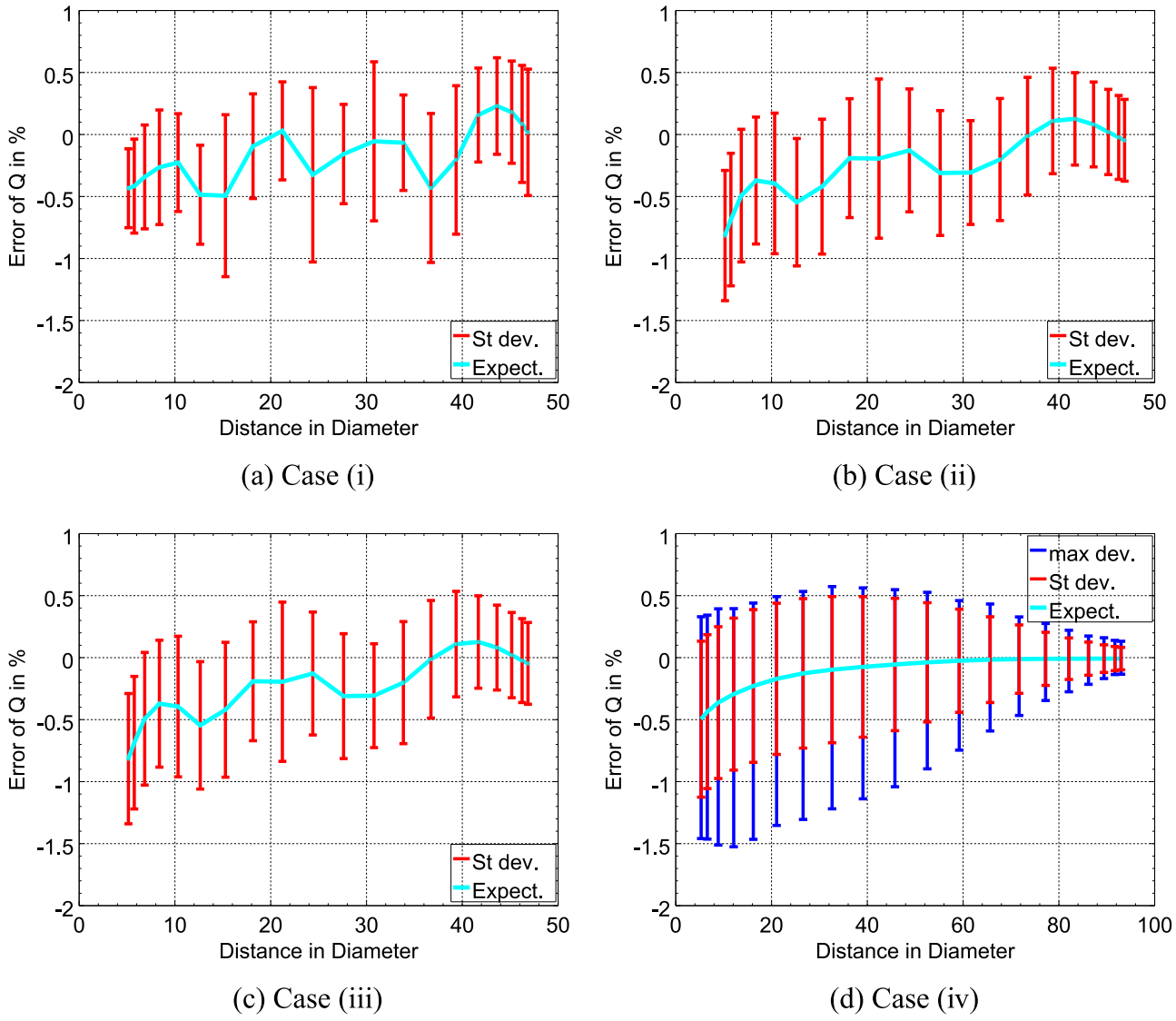


**Fig. 8.** The expected error of an EMFM and its standard deviation over the distance to the last elbow. For (a), (b) and (c): with a fixed angle of $\phi = 90°$ and the distance of the first double elbow as random variable with the same swirl direction (a), with the opposite swirl direction (b), both combined (c). The double elbow with fully developed inflow conditions with a random angular position of $\phi$ (d). The error bars in red denote the standard deviation, in blue the max and min deviation at each position. Note that the horizontal axis in (d) is twice as long as in the others. (For interpretation of the references to color in this figure caption, the reader is referred to the web version of this paper.)

predict the actual flow profile, because the inflow condition, which is in general unknown, also affects the resulting profile, as shown in Section 3. To determine the profile a second measurement technique can be installed for example to measure the wall shear stress as proposed by Wildemann [46] and applied by Ruppel [32,33] with pressure probes in the flange of a USFM. Also Yeh et al. [50] suggested a procedure to correct the measured flow rate of a USFM. For this several ultrasonic paths were necessary to achieve flow pattern recognition. Carlander and Delsing [6] drew a conclusion for self-diagnostics due to the turbulence of the measurement value of a USFM. There are also two patents [2,10] which claim to have a correction procedure for the USFM, depending on the distance of the last upstream disturbing installation. Further upstream disturbances are not included.

However, a simpler possibility is to disturb the flow directly in front of the measurement position in such a way that the shape of the axial velocity profile is stable and predictable for any inflow condition. For the USFM and the EMFM, the pipe diameter can be reduced with a nozzle right in front of the measurement device. This increases the flow velocity and straightens the flow profile which signifies a reduction in the asymmetry. However, the swirl will be enhanced, and another disadvantage is the head loss. In the following, the effect of a Venturi nozzle and a rectangular constriction with disturbed inflow conditions from a double elbow out-of-plane with varying distance are studied with the polynomial chaos method applied to CFD simulations. The two measurement principles of electromagnetic and ultrasonic flow meters were modeled as in Sections 4.1 and 5.1.

### 6.1. Venturi nozzle

Venturi nozzles can be used as flow meters due to the effect of pressure drop and its relation to the velocity. In addition, Venturi nozzles are also employed for flow homogenization. In this work we use the design of the new high temperature water flow standard at the Physikalisch-Technische Bundesanstalt (PTB) in Berlin, which is a Venturi nozzle with a diameter ratio of 0.5. It is used for laser optical LDV measurements, see [38,41]. Here, its geometry is considered in order to study the uncertainty of magnetic and ultrasonic flow meters inside the narrow part of the nozzle. A hexahedral mesh was generated consisting of 3.7 million elements and with dimensionless wall distance of $y^+ \approx 1$. The first step is to

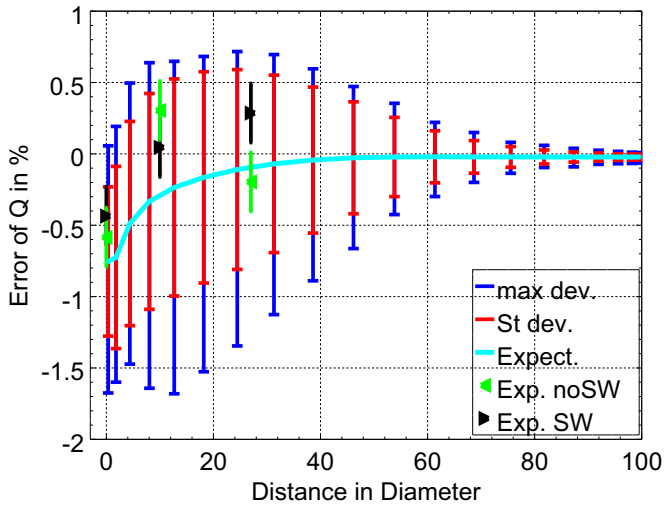


**Fig. 9.** The expected error of an EMFM over the distance. The double elbow with fully developed inflow conditions with a random angular position $\phi$. The red error bars denote the standard deviation, the blue ones the maximum and minimum values at each position downstream of the double elbow. The green and black triangles are the errors of measurement with an EMFM at FORCE[2] with standard deviation due to repeated measurements. (For interpretation of the references to color in this figure caption, the reader is referred to the web version of this paper).

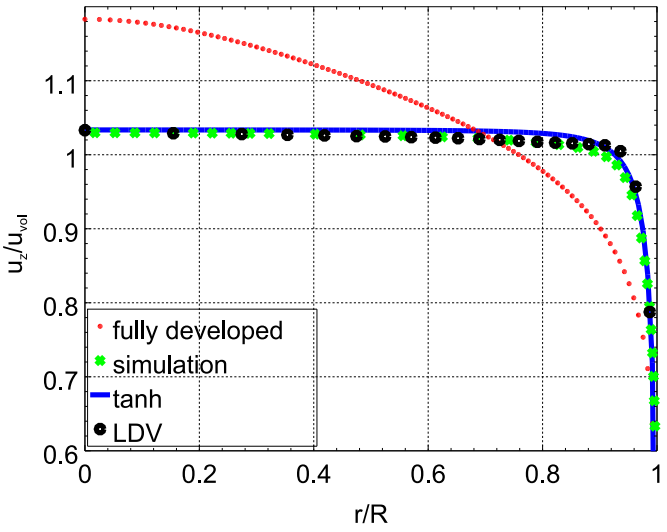


**Fig. 11.** Comparison of axis-symmetric flow profiles for a fully developed profile from Gersten [12] (red dots) and the profile inside the Venturi nozzle: simulation (green crosses), theoretical hyperbolic tangent profile (blue line) and LDV measurement data (black circles). (For interpretation of the references to color in this figure caption, the reader is referred to the web version of this paper.)

determine the flow profile in the Venturi nozzle for fully developed inflow conditions. In Fig. 11 the simulated profile is plotted in comparison with LDV measurements from PTB and a theoretical model based on a hyperbolic tangent approach, see [29,38]. Good agreement of the simulated data with both measurements and the theoretical profile can be obtained. Compared to the fully developed profile from Gersten [12], depicted in red dots, the profile in the Venturi nozzle is much flatter in the free stream region, while it is much steeper near the wall. The reference calibration factor $k$ for the ultrasonic and the magnetic flow meter can now be calculated for the new flow profile. For the USFM, $k_{USFM} = 0.988$ and for the EMFM $k_{EMFM} = 1.009$ ensued. As previously, the influence of disturbed inflow conditions on the velocity profile inside the Venturi is studied by application of the polynomial chaos approach. With a random upstream distance of the double elbow out-of-plane, the mean axial velocity profile inside the Venturi nozzle does not change significantly compared with a fully developed inflow profile. The standard deviation in the center area of the pipe is smaller than 0.3%. Near the wall, areas with deviations up to 1.6% appear, compare to Fig. 12a. The blue curve in Fig. 12b depicts the standard deviation for a single path from the center of the pipe to the pipe wall. Therefore, the angle was considered as a second random variable. The standard deviation is almost zero in the center point and increases moderately up to 0.3% until a radial position of $r/R \approx 0.9$. Closer to the wall the standard deviation increases rapidly up to 0.9% until it drops down to zero in the sublayer. The black curve is for fully developed inflow conditions with random path angle. Here, the standard deviation is almost zero until $r/R \approx 0.9$ and decreases until 0.3% near the wall. Consequently, even for an ideal inflow profile, an asymmetry appears inside the measurement section, which can be explained by the flow separation at the end of the narrow part. Nonetheless these deviations are quite small. The expected error and the standard deviation due to the random angular position of a flow meter over its distance to the double elbow are shown in Fig. 13. The maximum expected error of the flow rate measured by the USFM, shown in Fig. 13a, is $-0.2\%$ and decreases almost linearly to zero. The standard deviation (red error bars) decreases from about 1% to about 0.1%. The maximum and the minimum deviation (blue error bars) decrease from about 1.5% and $-2\%$ to less than $\pm 0.2\%$ respectively. The expected error for random angle and distance is

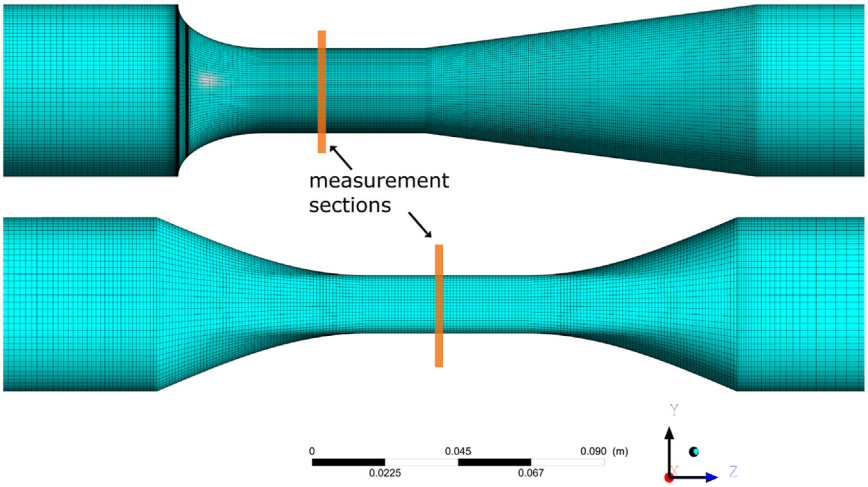


**Fig. 10.** The Venturi nozzle (top) and the rectangular restriction (bottom).

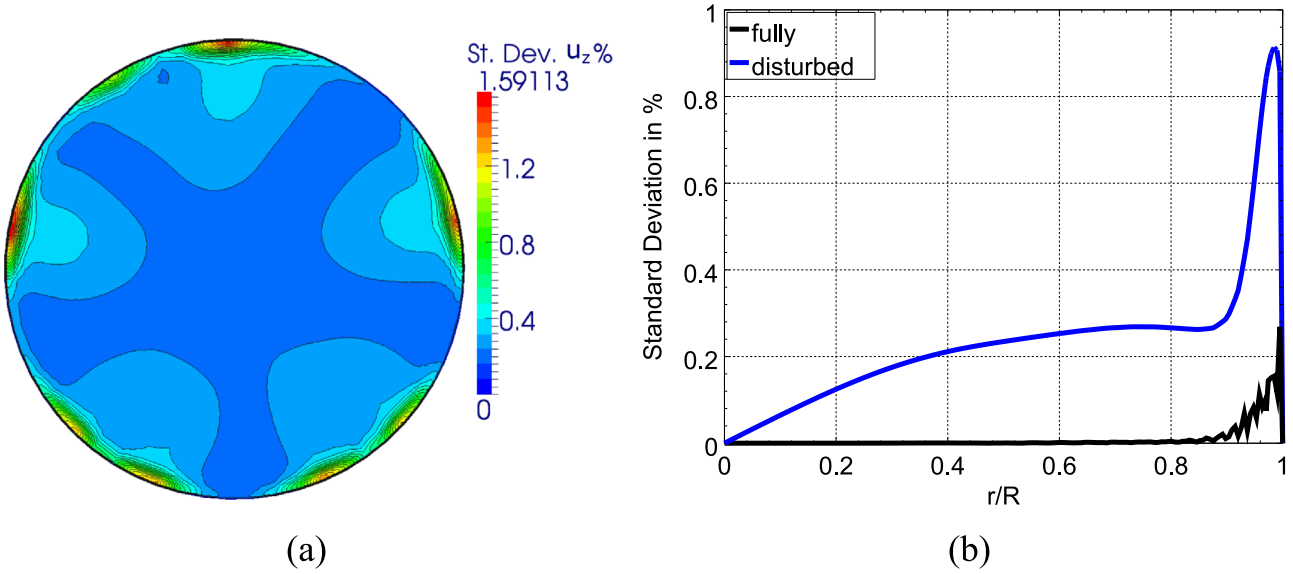


**Fig. 12.** Standard deviation in % of the velocity profile inside the Venturi nozzle. (a) For the measurement cross section and (b) of a single path with random angle $\phi$, for fully developed inflow conditions (black) and disturbed inflow conditions (blue). (For interpretation of the references to color in this figure caption, the reader is referred to the web version of this paper.)

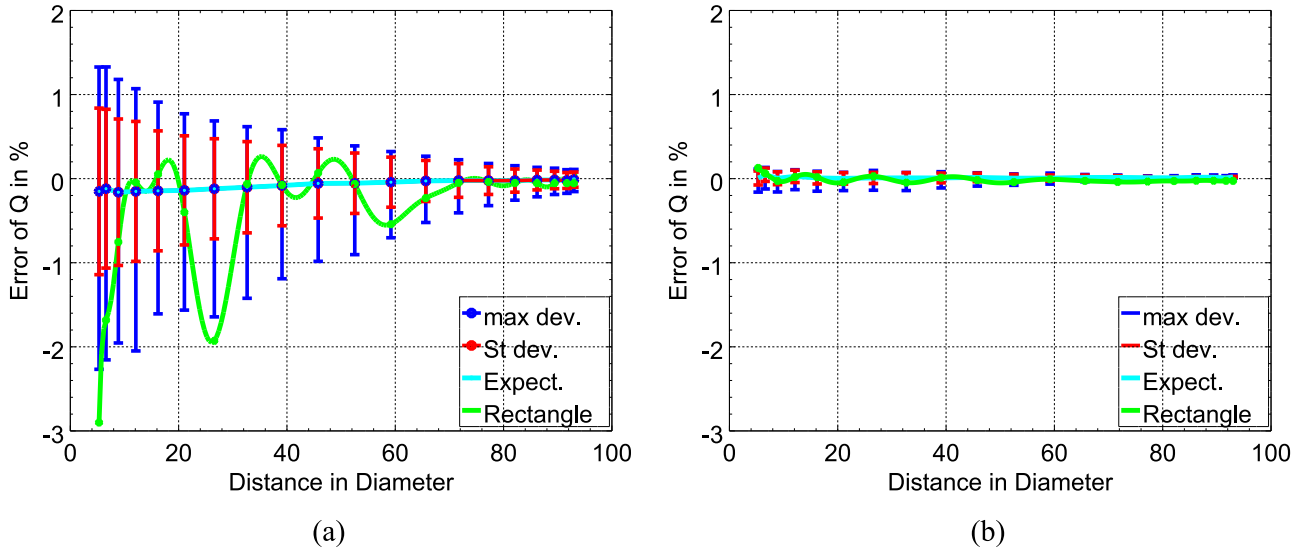


**Fig. 13.** The expected error of flow meters inside the Venturi constriction (cyan), their standard deviation (red) and the maximum/minimum deviation (blue) due to its random angular position $\phi$. The error in the rectangular constriction is with a fixed angular position $\phi$ (green). (a) for an USFM and (b) for an EMFM. (For interpretation of the references to color in this figure caption, the reader is referred to the web version of this paper.)

−0.11% with a standard deviation of 0.34%, compare to Table 2. Fig. 13b shows the results of the EMFM inside the Venturi nozzle. Here, the expected error as well as the standard deviation and the maximum/minimum deviations remain below 0.2% for all positions of the EMFM. The expected error for random angle and distance is −0.1% with a standard deviation of 0.02%, compare to Table 2.

The standard deviation in the Venturi nozzle is mostly driven by the secondary flow components. In the case without a constriction, mostly the asymmetry of the axial velocity profile is responsible for the errors. To illustrate this, the flow rates were calculated with Eq. (7), except that the secondary flow components $u_r$ and $u_\phi$ were set to zero. A comparison of the standard deviation is shown in Fig. 14. Without a constriction, the standard deviation with (red) and without (green) the non-axial flow components lies within the same range for distanced larger than 50$D$. For smaller distances it is about half a percent lower beforehand, except near a meter position of 5$D$ behind the double elbow, where the difference is even higher. For a measurement inside the Venturi nozzle, the influence of the non-axial flow components increases the standard deviation by a factor of 5, see the blue and cyan line.

### 6.2. Rectangular constriction

The rectangular constriction reduces the diameter of the straight pipe from $D=53.6$ mm in the $yz$-plane to $D_{yz}=18$ mm and in the $xz$-plane to $D_{xz}=46.5$ mm. The measurement section is modeled in the middle of the narrow part, see Fig. 10. The mesh consists of about 1.2 million hexahedrons, where the closest node to the wall has a dimensionless distance of $y^+ \approx 1$. As for the Venturi nozzle in the previous section, the inlet conditions were chosen to be the random distance of the double elbow out-of-plane. However, due to the non-symmetrical shape of the

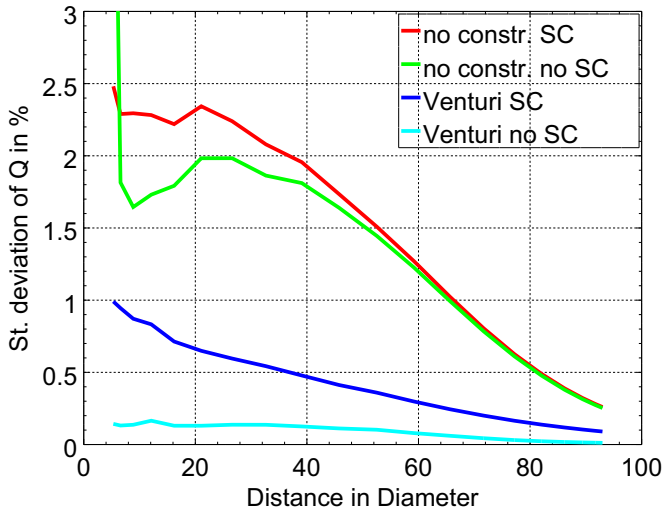


**Fig. 14.** Standard deviation in % of the flow rate Q for a USFM with random angular alignment over the distance to the last elbow. Without constriction, with the influence of secondary flow (red) and without secondary flow (green). Inside the Venturi nozzle with secondary flow components (blue) and without (cyan). (For interpretation of the references to color in this figure caption, the reader is referred to the web version of this paper.)

rectangular constriction the angular position $\phi$ of the flow meters is fixed. The ultrasonic beam is situated in the *yz*-plane, while the electromagnetic transducers are mounted in the *xz*-plane (the narrow side of the cross section). Similar to the approach in Section 6.1, reference calibration factors for the rectangular constriction have been obtained by an additional CFD simulation. The resulting factors are $k_{USFM} = 0.988$ for the USFM and $k_{EMFM} = 0.718$ for the EMFM, respectively. The results for the USFM show an oscillating error with decreasing amplitude towards zero, mostly in the negative area. Its error stays in most positions inside the standard deviation of the Venturi nozzle, but exceeds for $z/D=5$ and 25 for even the greatest errors of the Venturi, see Fig. 13a (green line). The overall expected error for random distance is −1.14%, its standard deviation is 1.12%, see Table 2. It seems, therefore, more sensitive to disturbed flow than the Venturi nozzle, even if it is hard to compare, because the angle of the meter was not varied. The error of an EMFM is also quite stable in the narrow part of the rectangular geometry. The error oscillates around zero and remains lower than 0.2% for all distances, see Fig. 13b (green line). The overall expected error for random distance to the disturbance is −0.1%, with a standard deviation of 0.01%, see Table 2. The uncertainty lies in the same scope as the Venturi nozzle.

It can be concluded that a diameter reduction in the form of a rectangular and a Venturi nozzle has great potential to reduce the error of a flow rate measurement downstream of disturbing installations. The diameter constriction particularly reduces the expected error in great amount. For EMFM the effect of disturbed flow conditions almost disappears.

## 7. Conclusion

Installations in the vicinity of flow meters are known to lead to systematic distortions of the measurement of flow rates. The main result of this paper is that computational fluid dynamics in combination with a recently developed technique for uncertainty quantification – the polynomial chaos method – is suitable to determine the bias $b$ and the systematic uncertainty contribution $u(b)$ for measurements with ultrasonic and electromagnetic flow meters. The "Guide to the expression of uncertainty in measurement" (GUM) [7] recommends strongly that measurement results are given as a combination of an output estimate $y$, and the associated uncertainty $u(y)$. The GUM demands further that known systematic biases $b$ are corrected by replacing $y$ by $y' = y + b$ and that uncertainty associated with the bias $b$ is added to the measurement uncertainty: $u'(y') = \sqrt{(u(y)^2 + u(b)^2)}$. Often $b$ and $u(b)$ cannot be obtained directly from the measurement. Here, we shown that flow simulation can be employed to determine the quantities $b$ and $u(b)$ and therefore enable a more reliable statement of the measurement result and its uncertainty. Our approach allows to us assess how the position of the flow meter and the installation of pipes upstream of it affect the magnitudes of $b$ and $u(b)$. In a second step, we also demonstrated how systematic effects can be partially compensated by additional elements such as Venturi nozzles and rectangular restrictions.

As far as industrial pipe and district heating systems are concerned, combinations of elbows are the most common pipe assemblies. Among the different pipe combinations, double elbows out-of-plane are of special interest, since they introduce strong disturbances into the flow profile and have a strong influence on many common types of flow meters. In front of a double elbow there is often another flow-disturbing installation. As a result the upstream conditions are unknown and an investigation of the resulting systematic bias on the measurement of the flow rate and the associated contribution to its measurement uncertainty is necessary. We demonstrate here that this can be achieved by a variation of the inlet profile in terms of swirls and asymmetry components.

It was shown that the axial flow profile, and also the strength of the swirl downstream of a double elbow out-of-plane, do not only depend on the geometry of the elbows, but are also strongly influenced by their inflow conditions. In particular, the azimuthal position of the profile varies with disturbed inflow conditions. Thus the angular position of an ultrasonic and an electromagnetic flow meter was modeled as a random variable in an uncertainty study of the meter performance. The expected flow rate is underestimated ($b < 0$), in most cases. The errors are higher the closer the meter is installed to the elbows. The standard deviation due to the random angular position is almost constant until about 40*D* downstream the elbows and decreases from there to almost zero at 100*D* distance. As the most influential parameters on the measured volume flow, the distance between the double elbow and the flow meter as well as the orientation of the flow meter were considered as random variables in the polynomial chaos approach. The resulting bias in the flow rate has been found to be in the range of 1.5–4.5% (0.1–0.5%) with a systematic uncertainty contribution of 2–2.4% (0.6–0.7%) of the respective flow rates for the ultrasonic (electromagnetic) flow meter if the distance to the double elbow is smaller than 40 pipe diameters. We emphasis that the systematic contribution to the uncertainty budget due to non-ideal inflow conditions is much higher than the contribution from the random errors imposed by the meter. For ultrasonic and electromagnetic flow meters random errors are typically lower than 0.1% for high Reynolds numbers [4,6].

If a constriction is placed directly in front of the meter the biases and uncertainties are substantially reduced. Therefore the flow meters were modeled in the narrow part of a Venturi nozzle and a rectangular constriction. The calibration factors were therefore adapted. For the ultrasonic flow meter the expected error can be reduced by more than one order of magnitude for the Venturi nozzle and 1.14% for the rectangular constriction, respectively. The Venturi nozzle decreases the standard deviation by a factor of two, in the rectangular constriction the standard deviation even increases. For an electromagnetic flow meter the expected errors inside the Venturi nozzle and the rectangular

constriction become quite small and can thus be neglected, as other effects in a real measurement like the instrument-related uncertainty contribution would be of higher magnitude.

## Contributorship statement

A. Weissenbrunner, A. Fiebach, and S. Schmelter developed the research idea. A. Weissenbrunner and A. Fiebach contributed equally to the drafting of the paper. M. Bär and T. Lederer wrote the research proposals, which secured the funding and provided the starting point for the research line in this paper. All authors contributed to the amendment of the manuscript.

## Acknowledgments

A. Weissenbrunner was supported by the Federal Ministry for Economic Affairs and Energy within the EnEff: Wärme project “On-site calibration of flow meters in district heating”. A. Fiebach and S. Schmelter were supported by the European Commission and EURAMET within the EMRP NEW-04 project “Novel mathematical and statistical approaches to uncertainty evaluation”.

The authors would like to thank Johan Bunde Kondrup from FORCE Technology, Ulrich Müller from Optolution Messtechnik GmbH, and our colleagues Jonas Steinbock and Markus Juling from PTB for their assistance and for providing the measurement data.

Supported by:

Federal Ministry for Economic Affairs and Energy

on the basis of a decision by the German Bundestag

## References

[1] N. Barton, CFD Simulation of Installation Effects for Electromagnetic Flowmeters, Report for National Measurement System Directorate Department of Trade & Industry, 2013.
[2] J. Baumoel, System and method for flow profile calibration correction for ultrasonic flowmeters, Patent, US 20090055119 A1, 2009.
[3] G. Bobovnik, J. Kutin, N. Mole, B. Stok, I. Bajsic, Numerical analysis of installation effects in coriolis flowmeters: a case study of a short straight tube full-bore design, Flow Meas. Instrum. 34 (2013) 142–150.
[4] O. Büker, Untersuchungen zur Darstellung und Weitergabe der Skala Volumen von Wasser mithilfe laseroptischer und konventioneller Messverfahren (Ph.D. thesis), TU Berlin, 2010.
[5] C. Carlander, J. Delsing, Installation effects on an ultrasonic flow meter, in: FLOMEKO, 1998, pp. 149–154.
[6] C. Carlander, J. Delsing, Installation effects on an ultrasonic flow meter with implications for self diagnostics, Flow Meas. Instrum. 11 (2000) 109–122.
[7] des Poids et Mesures, B.I.,électrotechnique internationale, C., internationale de normalisation, O., 1995. Guide to the Expression of Uncertainty in Measurement, International Organization for Standardization.
[8] T. Eichler, T. Lederer, Flow development behind a swirl generator in a hot-water standard measuring facility for large volume rates, Flow Meas. Instrum. 42 (2015) 89–97.
[9] R. Fedoryshyn, Y. Pistun, F. Matiko, V. Roman, Improvement of mathematical model of ultrasonic flowmeter for studying its errors in disturbed flows, in: Conference on Modelling Fluid Flow, 2015.
[10] T. Fröhlich, B. Kissling, Q. Müller, O. Berberig, K. Bussinger, Verfahren zur Ermittlung eines kompensierten Durchflusses und/oder einer kompensierten Strömungsgeschwindigkeit, Ultraschall-Durchflussmessgerät und Computerprogrammprodukt, Patent, DE 102013106108 A1, 2014.
[11] German Federal Ministry for Economic Affairs and Energy (BMWi), On-Site Calibration of Flow Meters in District Heating, URL ⟨http://www.eneff-stadt.info/en/new-technologies/project/details/on-site-calibration-of-flow-meters-in-district-heating/⟩, 2013.
[12] K. Gersten, Fully developed turbulent pipe flow, in: W. Merzkirch (Ed.), Fluid Mechanics of Flow Metering, Springer, Berlin, 2005, pp. 1–22.
[13] T. Gerstner, M. Griebel, Numerical integration using sparse grids, Numer. Algorithms 18 (3–4) (1998) 209–232.
[14] P. Guntermann, J. Rose, T. Lederer, M. Dues, U. Müller, A. Duckwe, In situ alibration of heat meters in operation, Euroheat & Power 8 (2011) 46–49.
[15] D.M. Halsey, Flowmeters in swirling flows, J. Phys. E: Sci. Instrum. 20 (1987) 1036–1040.
[16] J. Halttunen, Installation effects on ultrasonic and electromagnetic flowmeters: a model-based approach, Flow Meas. Instrum. 1 (1990) 287–292.
[17] A. Hilgenstock, R. Ernst, Analysis of installation effects by means of computational fluid dynamics, Flow Meas. Instrum. 7 (1996) 161–171.
[18] M. Holm, J. Stang, J. Delsing, Simulation of flow meter calibration factors for various installation effects, Measurement 15 (1995) 235–244.
[19] B. Horner, F. Mesch, An induction flowmeter insensitive to asymmetric flow profiles, in: M.S. Beck (Ed.), Process Tomography 1995, 6–8 April 1995, Bergen, Norway. UMIST, Manchester, 1995, pp. 321–330.
[20] S. Hosder, R.W. Walters, R. Perez, A non-intrusive polynomial chaos method for uncertainty propagation in CFD simulations, in: 44th AIAA Aerospace Science Meeting and Exhibit, American Institute of Aeronautics and Astronautics, Reno, Nevada, aIAA 2006-891, 9–12 January 2006.
[21] B. Iooss, C. Lhuillier, H. Jeanneau, Numerical simulation of transit-time ultrasonic flowmeters: uncertainties due to flow profile and fluid turbulence, Ultrasonics 40 (2002) 1009–1015.
[22] P.E. Kelner, 2007. Flow meter installation effects, in: American School of Gas Measurement Technology.
[23] J. Knourek, R. Matas, O. Prokes, D. Tenkrat, Numerical simulations of natural gas flow in pipe system with flowmeters, in: EPJ Web of Conferences, vol. 67, 2014, pp. 1–6.
[24] O.P. LeMaître, O.M. Knio, Spectral Methods for Uncertainty Quantification, Springer,, Dordrecht, 2010.
[25] O.P. Le Maître, O.M. Knio, H.N. Najm, R.G. Ghanem, A stochastic projection method for fluid flow. i. Basic formulation, J. Comput. Phys. 173 (2001) 481–511.
[26] O.P. Le Maître, M.T. Reagan, H.N. Najm, R.G. Ghanem, O.M. Knio, A stochastic projection method for fluid flow. ii. Random process, J. Comput. Phys. 181 (2002) 9–44.
[27] G.E. Mattingly, T.T. Yeh, Secondary flow effects due to several elbow configurations, in: ASME Fluid Measurement and Instrumentation Forum 1990, Toronto, Ontario, Canada, 4–7 June 1990.
[28] G.E. Mattingly, T.T. Yeh, Effects of pipe elbows and tube bundles on selected types of flow meters, Flow Meas. Instrum. 2 (1991) 4–13.
[29] B. Mickan, V. Strunck, A primary tandard for the volume flow rate of natural gas under high pressure based on laser doppler velocimetry, Metrologia 51 (2014) 459–475.
[30] B. Mickan, G. Wendt, R. Kramer, D. Dopheide, Systematic investigation of pipe flows and installation effects using laser doppler anemometry—Part ii. The effect of disturbed flow profiles on turbine gas meters—a describing empirical model, Flow Meas. Instrum. 7 (1996) 151–160.
[31] U. Müller, F. Adunka, M. Dues, P. Guntermann, J. Rose, T. Lederer, Möglichkeiten zur Vor-Ort-Überprüfung von großen Durchflusssensoren, Euroheat & Power 7-8 (2011) 52–55.
[32] C. Ruppel, Die intelligente Korrektur der Fehlerverschiebungen eines Ultraschall-Zählers bei gestörter Zuströmung (Ph.D. thesis), Universität Duisburg-Essen, 2003.
[33] C. Ruppel, F. Peters, How to correct the error shift of an ultrasonic flow meter downstream of installations, in: W. Merzkirch (Ed.), Fluid Mechanics of Flow Metering, Springer, Berlin, 2005, pp. 239–253.
[34] S. Schmelter, A. Fiebach, R. Model, M. Bar, Numerical prediction of the influence of uncertain inflow conditions in pipes by polynomial chaos, Int. J. Comput. Fluid Dyn. 29 (2015) 411–422.
[35] J.A. Shercliff, Relation between the velocity profile and the sensitivity of electromagnetic flowmeters, J. Appl. Phys. 25 (1954) 817–818.
[36] S.A. Smolyak, Quadrature and interpolation formulas for tensor products of certain classes of functions, Dokl. Akad. Nauk SSSR. 4 (1963) 123.
[37] C.C. Smyth, Derivation of weight functions for the circular and rectangular channel magnetic flowmeters, by means of Green's theorem and conformal mapping, J. Phys. E: Sci. Instrum. 4 (1971) 29–34.
[38] J. Steinbock, A. Weissenbrunner, M. Juling, T. Lederer, P.U. Thamsen, Uncertainty evaluation for velocity-area methods, Flow Meas. Instrum. 48 (2016) 51–56.
[39] K. Tawackolian, Fluiddynamische Auswirkungen auf die Messabweichung von Ultraschall-Durchflussmessgeräten (Ph.D. thesis), TU-Berlin, 2013.
[40] A. Weissenbrunner, T. Eichler, T. Lederer, Simulation einer Segmentblende und Vergleich mit PIV-Messungen, Fachtagung “Lasermethoden in der Strömungsmesstechnik”, 9–11 September 2014, Karlsruhe 22, 2014.
[41] A. Weissenbrunner, J. Steinbock, A. Fiebach, T. Lederer, Quantifizierung der Unsicherheit von Netzmessungen in einer Venturi-Düse bei unsicheren Zuströmbedingungen, in: Fachtagung “Lasermethoden in der Strömungsmesstechnik” 8–10 September 2015, Dresden, Germany, 2015.
[42] G. Wendt, T. Jahn, A. Hein, Investigation of flow behaviour of water in pipes and inside water meters and characterization of the flow by dimensionless parameters, in: International Workshop on Water and Heat Meters, 2013 (accessed 15.11.15).
[43] G. Wendt, B. Mickan, R. Kramer, D. Dopheide, Systematic investigation of pipe flows and installation effects using laser doppler anemometry—Part i. Profile

measurements downstream of several pipe configurations and flow conditioners, Flow Meas. Instrum. 7 (1996) 141–149.
[44] N. Wiener, The homogeneous chaos, Am. J. Math. 60 (1938) 897–936.
[45] D. Wilcox, 1986. Multiscale model for turbulent flows, in: AIAA 24th Aerospace Sciences Meeting, American Institute of Aeronautics and Astronautics.
[46] C. Wildemann, W. Merzkirch, K. Gersten, Correction of the reading of a flow meter in pipe flow disturbed by installation effects, in: W. Merzkirch (Ed.), Fluid Mechanics of Flow Metering, Springer, Berlin, 2005, pp. 224–237.
[47] W. Xiong, K. Kalkühler, W. Merzkirch, Measurement of velocity and turbulence downstream of flow conditioners, in: W. Merzkirch (Ed.), Fluid Mechanics of Flow Metering, Springer, Berlin, 2005, pp. 61–77.
[48] D. Xiu, Numerical Methods for Stochastic Computations: A Spectral Method Approach, Princeton University Press,, 2010.
[49] D. Xiu, G.E. Karniadakis, Modeling uncertainty in flow simulations via generalized polynomial chaos, J. Comput. Phys. 187 (2003) 137–167.
[50] T.T. Yeh, P.I. Espina, S.A. Osella, An intelligent ultrasonic flow meter for improved flow measurement and flow calibration facility, in: IEEE Intrumentation and Measurement Technology Conference, 2001.
[51] T.T. Yeh, G.E. Mattingly, Laser Doppler Velocimeter Studies of the Pipeflow Produced by a Generic Header, NIST Technical Note 1409, 1995, pp. 1118–1139.
[52] T.T. Yeh, G.E. Mattingly, Flowmeter Installation Effects due to a Generic Header, Technical Note 1419, National Institute of Standards and Technology, 1996.
[53] T.T. Yeh, G.E. Mattingly, Computer simulations of ultrasonic flow meter performance in ideal and non-ideal pipe flows, in: ASME Fluids Engineering Division Summer Meeting FEDSM, 1997.